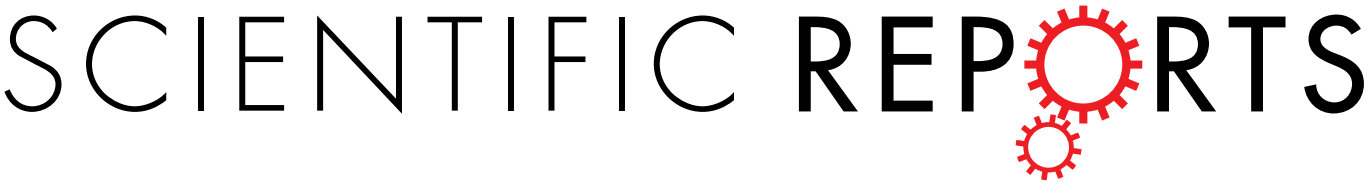

OPEN

First-principles calculated decomposition pathways for $LiBH_4$ nanoclusters

Received: 07 December 2015
Accepted: 25 April 2016
Published: 18 May 2016

Zhi-Quan Huang[1,*], Wei-Chih Chen[1,*], Feng-Chuan Chuang[1], Eric H. Majzoub[2] & Vidvuds Ozoliņš[3]

We analyze thermodynamic stability and decomposition pathways of $LiBH_4$ nanoclusters using grand-canonical free-energy minimization based on total energies and vibrational frequencies obtained from density-functional theory (DFT) calculations. We consider $(LiBH_4)_n$ nanoclusters with $n = 2$ to 12 as reactants, while the possible products include $(Li)_n$, $(B)_n$, $(LiB)_n$, $(LiH)_n$, and $Li_2B_nH_n$; off-stoichiometric $Li_nB_nH_m$ ($m \leq 4n$) clusters were considered for $n = 2$, 3, and 6. Cluster ground-state configurations have been predicted using prototype electrostatic ground-state (PEGS) and genetic algorithm (GA) based structural optimizations. Free-energy calculations show hydrogen release pathways markedly differ from those in bulk $LiBH_4$. While experiments have found that the bulk material decomposes into LiH and B, with $Li_2B_{12}H_{12}$ as a kinetically inhibited intermediate phase, $(LiBH_4)_n$ nanoclusters with $n \leq 12$ are predicted to decompose into mixed Li_nB_n clusters via a series of intermediate clusters of $Li_nB_nH_m$ ($m \leq 4n$). The calculated pressure-composition isotherms and temperature-pressure isobars exhibit sloping plateaus due to finite size effects on reaction thermodynamics. Generally, decomposition temperatures of free-standing clusters are found to increase with decreasing cluster size due to thermodynamic destabilization of reaction products.

Hydrogen is a promising next-generation energy carrier due to its high energy density, high energy conversion efficiency, and absence of harmful emissions. However, on-board hydrogen storage is still a serious challenge for developing economically viable hydrogen-powered passenger vehicles[1]. To achieve widespread commercialization, hydrogen storage systems should simultaneously possess several characteristics such as safety, high gravimetric and volumetric densities, fast reversible hydrogen release and uptake under moderate pressures and temperatures matched to the operating conditions of proton exchange membrane (PEM) fuel cells.

Complex metal hydrides emerged as feasible high-density hydrogen storage materials after Bogdanović and Schwickardi demonstrated reversible (de)hydrogenation reactions in transition metal doped sodium alanate ($NaAlH_4$)[2]. Spurred by this discovery, many other complex hydrides have been explored as candidate hydrogen storage materials, including alanates, amides, and borohydrides. Lithium borohydride, $LiBH_4$, has received particular attention owing to its high gravimetric (18.5 wt.% H_2) and volumetric (121 g H_2/L) densities. However, due to its high thermodynamic stability and slow kinetics, hydrogen release from bulk $LiBH_4$ requires very high temperatures that are incompatible with proton-exchange membrane (PEM) fuel cells[3–5]. In addition, the tendency to release diborane during dehydrogenation leads to irreversibility and causes poisoning of the fuel cell[6–10].

Destabilization has been extensively explored as a means of improving the thermodynamics of hydrogen storage reactions[11–14]. The main idea of this approach is to add a second reactant, which upon decomposition forms a stable low-energy product phase and lowers the overall reaction enthalpy. The canonical example of a destabilized reaction is $LiBH_4 + MgH_2 \rightarrow LiH + MgB_2 + (5/2)H_2$, where the addition of MgH_2 leads to the formation of MgB_2 as a low-energy product phase. This significantly lowers the reaction enthalpy relative to the decomposition reaction of the pure compound, $LiBH4 \rightarrow LiH + B + (3/2)H_2$. Unfortunately, destabilization is not very effective in lowering the *kinetic* barriers to hydrogen release, leading to only modest improvement in the hydrogen release temperatures.

[1]Department of Physics, National Sun Yat-Sen University, Kaohsiung 804, Taiwan. [2]Center for Nanoscience and Department of Physics and Astronomy,University of Missouri-St. Louis, St. Louis, Missouri 63121, United States. [3]Department of Materials Science and Engineering, University of California Los Angeles, Los Angeles, California 90095-1595, USA. *These authors contributed equally to this work. Correspondence and requests for materials should be addressed to F.C.C. (email: fchuang@mail.nsysu.edu.tw) or V.O. (email: vidvuds@ucla.edu)

Another approach to improving the thermodynamics and kinetics of hydrogen release consists of using $LiBH_4$ nanoparticles incorporated in support materials with nanoscale pores, such as nanoporous carbon or metal-organic frameworks (MOFs)[9,10,15–24]. Besides improving the kinetics and lowering the temperature of hydrogen release, this strategy has also been shown to suppress the formation of diborane[19,25,26]. First-principles density-functional theory (DFT) based studies[27,28] have investigated the thermodynamic properties of nano-$LiBH_4$, suggesting that bonding with the nanoporous carbon support plays a key role in improving the thermodynamic properties of nano-$LiBH_4$. However, due to the large configuration space, these studies did not perform comprehensive examination of the most stable cluster structures and compositions as functions of cluster size. Hence, a complete picture of the size-dependent thermodynamics properties of $LiBH_4$ nanoparticles and their decomposition products is not yet available.

Decomposition pathways and pressure-composition isotherms are determined using free energy minimization in the grand canonical ensemble[29]. In addition to clusters with the chemical composition of bulk $LiBH_4$ and its predicted bulk decomposition products $Li_2B_{12}H_{12}$, LiH and B[30], we considered $(Li)_n$, $(LiB)_n$, and $Li_2B_nH_n$ clusters as possible products. To assess the role of other cluster compositions, further detailed studies were performed for the decomposition reactions of $(LiBH_4)_2$, $(LiBH_4)_3$ and $(LiBH_4)_6$ including $Li_2B_2H_n$ ($n = 1$ to 7), $Li_3B_3H_n$ ($n = 1$ to 11) and $Li_6B_6H_n$ ($n = 1$ to 23) clusters as possible intermediate products. Our analysis shows that the reaction end products are changed from $(LiH)_n + B_n + (3/2)H_2$ to $(LiB)_n + 2nH_2$ when the size of reactants is reduced to the nanoscale. The calculated reaction enthalpies decrease from 238 ($n = 2$) to 133 kJ/mol H_2 ($n = 12$) with increasing cluster size, remaining significantly above the bulk decomposition enthalpy of $LiBH_4$. The hydrogen release temperatures are predicted to behave in a non-trivial way, with multiple intermediates appearing in the simulated dehydrogenation processes. The finite size effects and presence of intermediates manifest in multiple plateaus in the calculated release curves as functions of temperature, while the calculated pressure-composition isotherms and temperature-composition isobars exhibit sloping plateaus. Our study provides an in-depth understanding of the thermodynamics of hydrogen release from nanoscale particles and shows the importance of engineering appropriate support materials that can bind the reaction products and lower the reaction enthalpies to achieve reversible hydrogen storage in a practically viable range of temperatures and pressures.

Results

Structure of reactants and products. We start by briefly describing our findings for the atomic geometries of the reactants and products, which are summarized in Fig. 1. The reactants, $LiBH_4$ nanoclusters, are composed of the cation, Li^+, and the anionic group, BH_4^-. We find that the lowest energy conformations of small $(LiBH_4)_n$ clusters are chainlike, forming closed rings. The tetrahedral BH_4^- anion is a near perfect tetrahedron in all cases with some elongation in the B-H bond length from 1.22 to 1.24 Å. Note that the length of the B-H bond in bulk $LiBH_4$ is 1.22 Å. The diameter of $LiBH_4$ clusters increases gradually from 6.0 to 10.4 Å upon increasing the cluster size from $n = 2$ to 12. $(LiH)_n$ clusters form rocksalt-derived structures for sizes $n \geq 4$.

For boron clusters, our GA method reproduced the lowest energy structures found in earlier studies[31–33]. Small boron clusters are found to form 2-dimensional planar structures except for the B_9 cluster which has two boron atoms on two sides of the circular substructure with seven boron atoms forming a ring. Changes in the cluster geometries with increasing number of boron atoms indicate that boron nanoclusters prefer to have a coordination number of six.

For pure lithium clusters, the GA again finds the same structures as those in previous studies[34,35]. Unlike boron clusters, lithium clusters agglomerate in three-dimensional motifs when the the cluster sizes exceed four atoms.

In the mixed lithium-boron clusters $(LiB)_n$, the boron atoms generally tend to gather in the center of the cluster with lithium atoms surrounding them on the periphery. In addition, for $n \leq 5$ the arrangement of boron atoms is the same as in the pure boron clusters. When $n > 5$, boron atoms in the center are distorted due to interactions with the surrounding lithium atoms. We also found that the B-B distances in the center of the $(LiB)_n$ clusters are gradually increased from 1.53 Å for $n = 2$ to 1.85 Å for $n = 12$, while the Li-B bond lengths stay approximately constant. It appears that interactions with the outer Li ions and charge transfer from Li to B combine to push the B atoms outward.

Cluster energies. To better understand the thermodynamic stability, reaction pathways and reaction enthalpies, we first discuss the cluster-size dependent energetics of reactants and reaction products. Figure 2 shows the relative energies of clusters normalized by their bulk energies without the zero-point energy (ZPE) corrections. This quantity is defined as the ratio of the energy of the cluster per formula unit versus the energy of the bulk phase. Bulk lithium is calculated in the $Im\bar{3}m$ body-centered cubic lattice, bulk boron is in the α-B phase, and bulk LiH is in the rocksalt structure. Bulk $LiBH_4$ has several near-degenerate ground-state structures[36], and the *Pnma* structure is used in our calculations[37]. As for bulk LiB, we used a $P6_3/mmc$ structure reported in a previous experimental study[38]. The calculated reaction enthalpy for the decomposition of bulk $LiBH_4$ at $T = 0$ K is $\Delta H = 60$ kJ/(mol H_2) with zero-point energy (ZPE) corrections, while excluding ZPE we obtain 82 kJ/(mol H_2). The predicted decomposition temperature is $T_{dec} = 340$ °C at $p = 1$ bar hydrogen pressure, which is about 100 °C below experimental results. We find that the stabilities of the reaction products are dramatically reduced with decreasing cluster size, with LiH and LiB clusters being more stable than pure Li and B clusters. However, the behavior of the reactant $LiBH_4$ clusters is very different: the energy per formula unit of $(LiBH_4)_n$ is nearly flat from $n = 2$ to $n = 12$, which signals that their thermodynamic stability is reduced only slightly upon decreasing cluster size. This suggests that most of the binding energy is stored in the polar covalent B-H bonds, while the electrostatic interactions between lithium and BH_4^- complexes are relatively weak. Examination of the size-dependent stabilities of each cluster type shows that clusters with even-numbered formula units are generally more stable than the odd ones. For pure clusters, Li_n and B_n, we find that Li_3, Li_5, Li_9, Li_{11}, B_7, B_9, and B_{11} possess certain geometric symmetries, but they are unstable with respect to decomposition into even-numbered $n + 1$ and $n - 1$

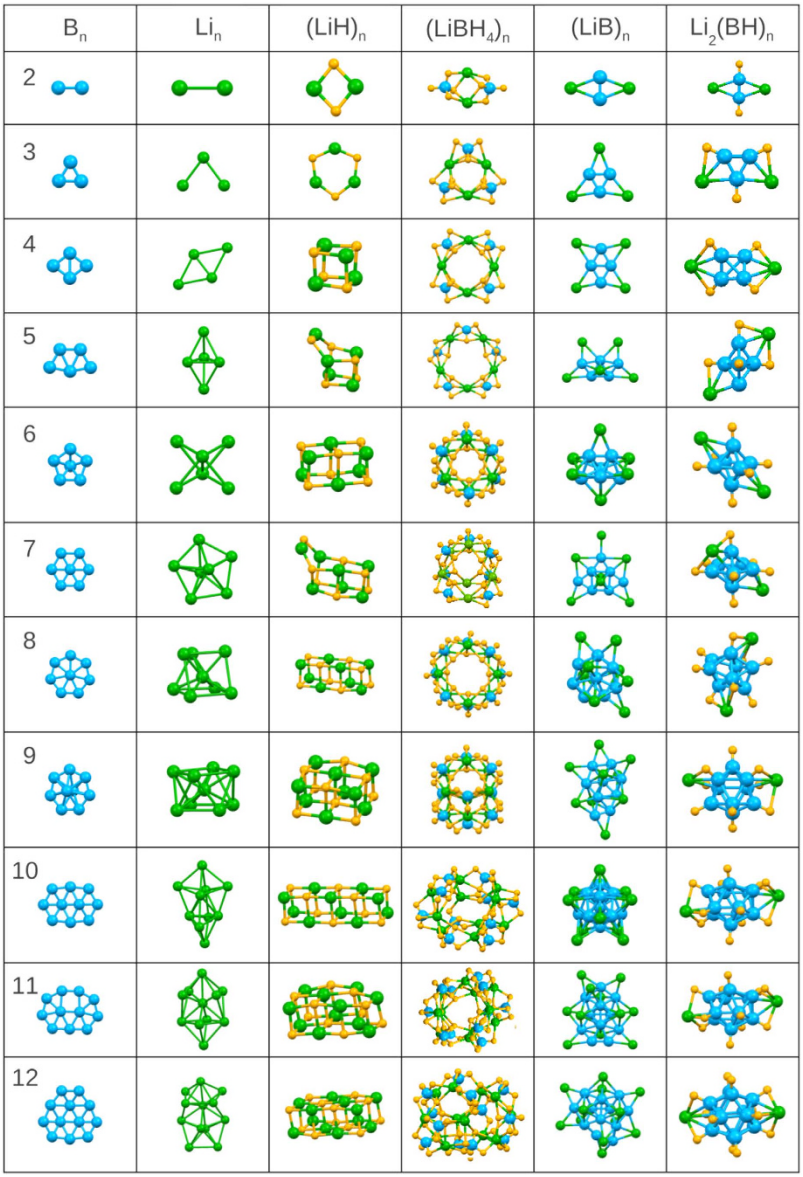

Figure 1. First-principles relaxed cluster geometries found in this work. B, Li, and H atoms are the blue, green and yellow spheres, respectively.

clusters due to unpaired electron filling in the highest occupied molecular orbital. As for the LiH and LiB clusters, even though the highest orbitals in $(LiH)_5$, $(LiH)_7$, $(LiH)_{11}$, and $(LiB)_9$ are fully occupied, these clusters are unstable because of broken geometric symmetry. Moreover, $(LiH)_{10}$ and $(LiB)_5$ are also unstable because they are at the structural transition point between distinct bonding topologies.

Decomposition pathways of $LiBH_4$ clusters. Previous computational work[30] has shown that, thermodynamically, decomposition of bulk $LiBH_4$ should occur via the formation of an intermediate closoborane $Li_2B_{12}H_{12}$ compound. However, the formation of closoboranes is kinetically inhibited in experiments and decomposition proceeds directly to a mixture of LiH and B. We begin our discussion of the decomposition pathways of $LiBH_4$ nanoclusters by considering simplified decomposition reactions with closoborane $Li_2B_nH_n$, elemental $(Li)_n$ and $(B)_n$, and binary $(LiH)_n$ and $(LiB)_n$ clusters as the end products; the full treatment using the ensemble grand canonical formalism is given below. First, we consider the following reaction pathways:

$$(LiBH_4)_n \rightarrow (LiH)_n + B_n + \frac{3n}{2}H_2, \tag{1}$$

$$(LiBH_4)_n \rightarrow Li_n + B_n + 2nH_2, \tag{2}$$

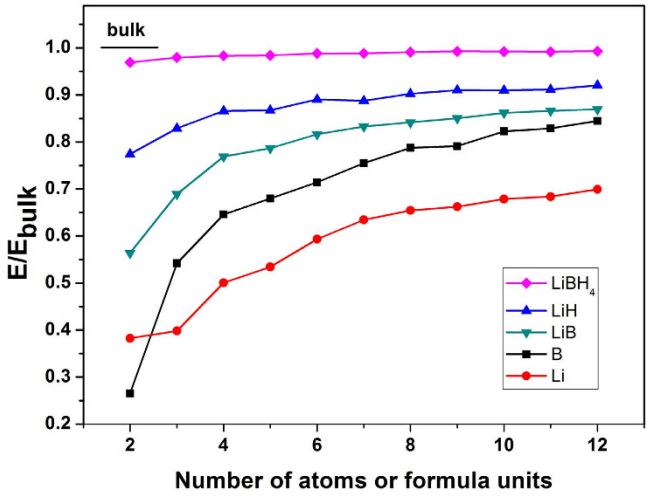

Figure 2. Calculated DFT total energies (without zero-point energy corrections) of $(LiBH_4)_n$, $(LiH)_n$, $(LiB)_n$, B_n and Li_n clusters, normalized to the corresponding bulk values.

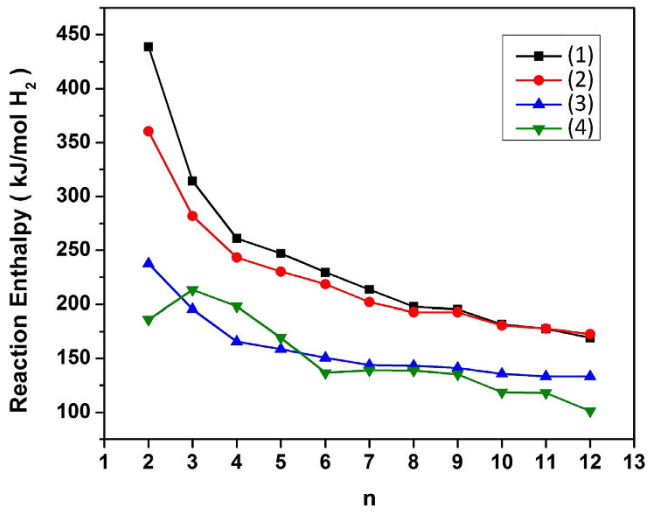

Figure 3. Calculated DFT reaction enthalpies(without ZPE correction) of the four decomposition pathways of nano-$LiBH_4$ given by Eqs 1–4, shown as functions of the cluster size *n*.

$$(LiBH_4)_n \rightarrow (LiB)_n + 2nH_2, \tag{3}$$

$$(LiBH_4)_n \rightarrow Li_2B_nH_n + (LiH)_{n-2} + (n+1)H_2. \tag{4}$$

Equations 1 and 2 are the nanocluster analogues of the bulk decomposition reactions occurring at $T = 400$ and 900 °C, respectively[3]. Reaction 4 is the nanocluster analogue of the bulk decomposition reaction into $Li_2B_{12}H_{12}$, accounting for the formation of various closoborane $(B_nH_n)^{2-}$ species with $n \leq 12$, while the product of Eq. 1 can be obtained by further decomposition of a mixture of $Li_2B_nH_n$ and $(LiH)_{n-2}$. Finally, Eq. 3, is similar to the favored decomposition reaction predicted for nano-$NaAlH_4$[29].

The calculated DFT reaction enthalpies of Eqs 1–4 without vibrational free energy contributions are shown in Fig. 3. In all cases, the calculated DFT reaction enthalpies are larger than the decomposition enthalpy of bulk $LiBH_4$ [82 kJ/(mol H_2)]. This does not mean that $LiBH_4$ nanoclusters are generally more stable with respect to decomposition than the bulk compound because these data are based on a limited number of possible reactions and reaction products; we will show below that the Gibbs free energy minimization approach and inclusion of product clusters with intermediate hydrogen content can lower the reaction enthalpies significantly. The trend towards higher reaction enthalpies for the hypothesized reactions in Eqs 1–4 can be easily explained from the size-dependence of the cluster binding energies in Fig. 2: since the $(LiBH_4)_n$ clusters show weak size dependence, while all the product clusters show much stronger finite size energy penalty, the reaction enthalpies are significantly higher than the bulk limit. It is interesting to note that of all four reaction pathways, the bulk-like Eq. 1 is

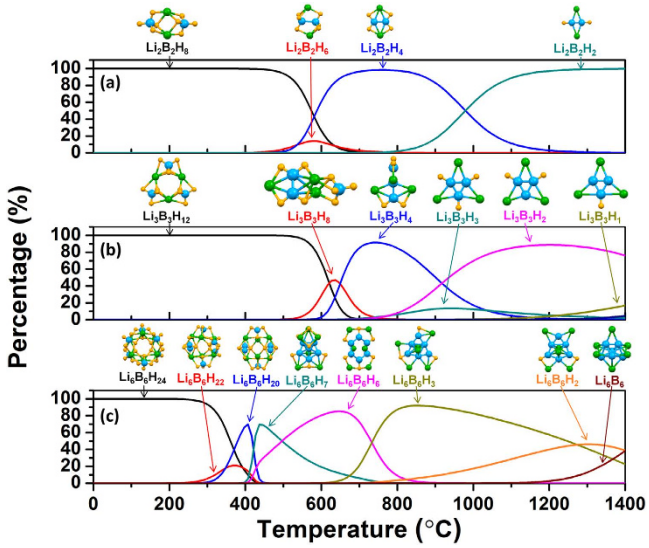

Figure 4. Calculated decomposition pathways of (**a**) $(LiBH_4)_2$, (**b**) $(LiBH_4)_3$, and (**c**) $(LiBH_4)_6$ nanoclusters obtained from Gibbs free energy minimization, Eqs S1–S3. Lithium, boron and hydrogen atoms are shown as green, blue, and yellow spheres, respectively.

the least favorable one in nano-$LiBH_4$, which shows that the reaction path can change dramatically upon reducing the particle size to the nanometer regime; similar effects have been predicted for sodium alanate[29,39]. Both pathways in Eqs 2 and 3 liberate all the hydrogen, and our results show that Eq. 3 is more favorable than Eq. 2 because the binary $(LiB)_n$ clusters are more stable than the mixture of $(Li)_n$ and $(B)_n$ clusters. We note that the formation of $Li_2B_nH_n$ clusters via Eq. 4 is the preferred path for $n = 6$ to 12 when closoborane species form as the end product, while the pathway in Eq. 3 is preferred for n = 3 to 5. In general, we find that the calculated reaction enthalpies decrease with increasing cluster size n, and are significantly higher than the calculated DFT enthalpies for decomposition of bulk-$LiBH_4$ into $Li_2B_{12}H_{12}$[30]. Due to the high stability of $B_{12}H_{12}^{2-}$ complex anions, the reaction enthalpy of Eq. 4 drops significantly from $n = 11$ to $n = 12$, and one may expect that these species will persist as the dominant end product for $n > 12$.

To investigate the possibility that intermediate products other than those in Eqs 1–4 may form during decomposition, we have carried out calculations for clusters with the general formula $Li_nB_nH_m$, where $0 < m < 4n$ and $n = 2$, 3, and 6. For this series, we adopted the random search scheme rather than the genetic algorithm. The random search scheme is implemented as follows. New initial structures were randomly generated by removing one or more H atoms from nano-$LiBH_4$ and by gradually adding H atoms to LiB nanoclusters, breaking symmetries by slightly distorting all atoms away from the original positions. These randomly generated structures were then relaxed using DFT forces to a local minimum configuration, and the energies of the most favorable structures at each composition were used in the Gibbs ensemble formalism given by Eqs S1–S3 (See Supplementary Information). The zero point energy, temperature-dependent vibrational free energy, and the free energy of the diatomic H_2 gas are included in these calculations. Our results for the cluster type fractions p_f are summarized in Fig. 4 assuming a hydrogen pressure of $p = 0.01$ bar, which is representative of experimental measurements.

Figure 4(a) shows the calculated dehydrogenation pathway of $(LiBH_4)_2$ and the structures of the predicted intermediate products as functions of temperature. $(LiBH_4)_2$ nanoclusters start to release hydrogen at approximately 450 °C by first forming $Li_2B_2H_6$. The structure of this cluster resembles diborane, with a significant difference that the donation of two electrons from Li atoms reconfigures the three-center two-electron bonds of diborane into a direct B-B bond. At 500 °C, $Li_2B_2H_4$ clusters form and exist as the dominant specie from 580 to 980 °C. Finally, $Li_2B_2H_2$ clusters appear at 800 °C and dominate until full dehydrogenation into $(LiB)_2$ as the end product above 1400 °C (not shown). We note that the intermediate products in the dehydrogenation pathway of $(LiBH_4)_2$ all contain an even number of hydrogen atoms, and each intermediate reaction step releases one H_2 molecule per cluster.

Figure 4(b) shows the decomposition pathway of $(LiBH_4)_3$. It is seen that hydrogen release starts at 530 °C where two H_2 molecules per cluster are released to form $Li_3B_3H_8$, which exists in a narrow temperature interval. The latter cluster is essentially a superposition of $Li_2B_2H_4$ and $(LiBH_4)_1$ clusters, which explains its marginal stability. In the next step, two more H_2 molecules are released to form $Li_3B_3H_4$, bypassing $Li_3B_3H_6$ entirely. At temperatures of 920 °C and higher, a $Li_3B_3H_2$ cluster is formed by releasing another H_2 molecule, before full dehydrogenation to the end product Li_3B_3. Small fraction of $Li_3B_3H_3$ and $Li_3B_3H_1$ clusters with odd-numbered hydrogen atoms is predicted to appear intermittently.

Finally, Fig. 4(c) shows the dehydrogenation pathway of $(LiBH_4)_6$. Even-numbered $Li_6B_6H_{22}$ and $Li_6B_6H_{20}$ clusters stage a brief appearance at 250 and 300 °C, respectively. The structures of these clusters can be described as derived from the parent borohydride cluster by releasing a hydrogen molecule and forming a $B_2H_6^{2-}$ complex anion. It is tempting to hypothesize that $2BH_4^{2-} \rightarrow B_2H_4^{2-}$ also represents a *kinetically* viable hydrogen release

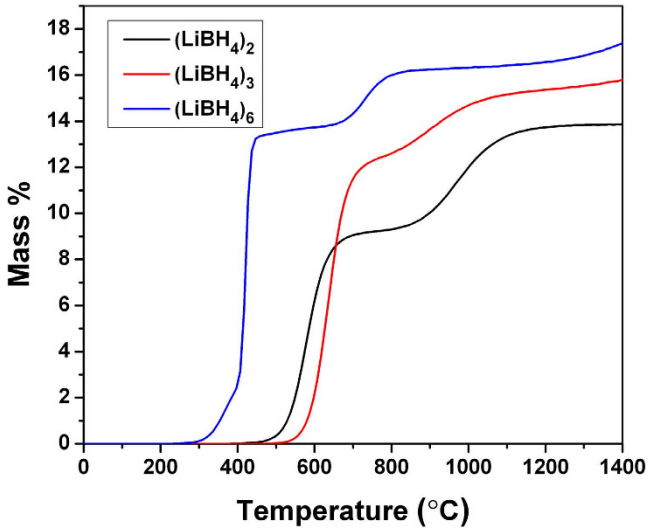

Figure 5. Mass fraction of released hydrogen as a function of temperature at constant hydrogen pressure $p = 0.01$ bar.

pathway, but this has to be verified by separate studies of the activation energies. In any case, the negative charge carried by the BH_4^- anions should present a significant barrier to bringing these complexes together for the reaction. Most of the hydrogen is released around 420 °C with the appearance of $Li_6B_6H_7$ and $Li_6B_6H_6$ clusters. The latter cluster exhibits a high degree of symmetry and appears to be stable over a wide range of temperatures up to approximately 700 °C. In the final reaction steps, $Li_6B_6H_3$, $Li_6B_6H_2$ and Li_6B_6 show up one by one as the majority cluster phases. Again, it is seen that most of the stable clusters in the decomposition sequence contain an even number of hydrogen atoms, with the brief appearance of $Li_6B_6H_7$ as the only exception.

Based on the data in Fig. 4, we have calculated the cumulative mass fraction of released H_2 as a function of temperature at constant pressure (i.e., temperature-composition isobar). Figure 5 shows the results of these calculations. It is seen that the calculated hydrogen release curves exhibit nontrivial behavior as functions of temperature and cluster size.

For instance, the initial onset of hydrogen release occurs at a lower temperature for the $n = 2$ cluster than for the $n = 3$ cluster. This is due to the fact that the $n = 2$ cluster can release one H_2 molecule and form $Li_2B_2H_6$ (which consists of two Li^+ ions and a $B_2H_6^{2-}$ anion), while the corresponding $Li_3B_3H_{10}$ compound is unfavorable because it involves a mixture of $B_2H_6^{2-}$ and BH_4^- anions. Furthermore, all three clusters exhibit two sloping plateaus in their dehydrogenation curves. Focusing on the $n = 6$ cluster, most of the hydrogen comes off in a narrow temperature interval before the first plateau, corresponding to successive removal of hydrogen molecules and eventual formation of $Li_2B_6H_6$ with an overall formula Eq. 4. In the second stage, a smaller amount of hydrogen is released by decomposing $Li_2B_6H_6$ and forming $Li_2B_6H_3$, etc. With increasing cluster size of nano-$LiBH_4$, we expected that the amount of hydrogen released in the first-stage will increase and that the main hydrogen release step will shift to lower temperatures. According to the reaction enthalpies in Fig. 3, the overall reaction for $n \leq 12$ is expected to proceed according to Eq. 4, even though it seems likely that the full pathway will consist of multiple intermediate steps, similar to those discussed above. For $n > 12$, we hypothesize that the formation of clusters with Li-compensated $B_mH_m^{2-}$ complex anions ($6 \leq m \leq 12$) will be favorable, but the existence of intermediate steps is also likely, in a manner similar to the $n = 6$ case. Unfortunately, reliable structure prediction for such large systems is beyond the capabilities of current computational methods.

Due to the increased enthalpy difference between the reactants and products, to achieve dehydrogenation at the same pressure as bulk $LiBH_4$, $(LiBH_4)_6$ nanoclusters need temperatures that are approximately 200 °C higher. Since experimental measurements on nanoconfined borohydrides[18–20] often find lowering of the desorption temperature, this indicates that the supporting substrate plays an important role by binding the supported nanoclusters and lowering the enthalpy of the reaction products relative to $(LiBH_4)_n$.

While dehydrogenation is usually carried out by increasing temperature at a constant pressure, as shown in Figs 4 and 5, hydrogen absorption measurements are commonly done by increasing pressure at constant temperature. Hence, pressure-composition isotherms (PCT), showing the equilibrium pressure of the H_2 gas coexisting with a material with a given the hydrogen content, are of considerable interest. For bulk materials, these curves show flat regions corresponding to equilibria between the hydrogen gas and two solid phases on the opposite sides of the miscibility gap. In nanomaterials, clusters with different hydrogen content play the role of the coexisting solid phases. However, in contrast to bulk systems where the plateaus are perfectly flat in the thermodynamic limit with no kinetic limitations, in finite size clusters the plateaus acquire slope. This is illustrated in Fig. 6, which shows the calculated DFT pressure-composition isotherms for $(LiBH_4)_6$ clusters at three different temperatures. The left-hand side is the dehydrogenated phase, $Li_6B_6H_6$, corresponding 4.6 wt.% H_2 on the horizontal axis. The fully hydrogenated phase, $(LiBH_4)_6$ is on the right-hand side, at 18.5 wt.% H_2. Going right-to-left, the sloping plateaus describe the series of increasingly hydrogen-poor clusters in the decomposition sequence of $(LiBH_4)_6$,

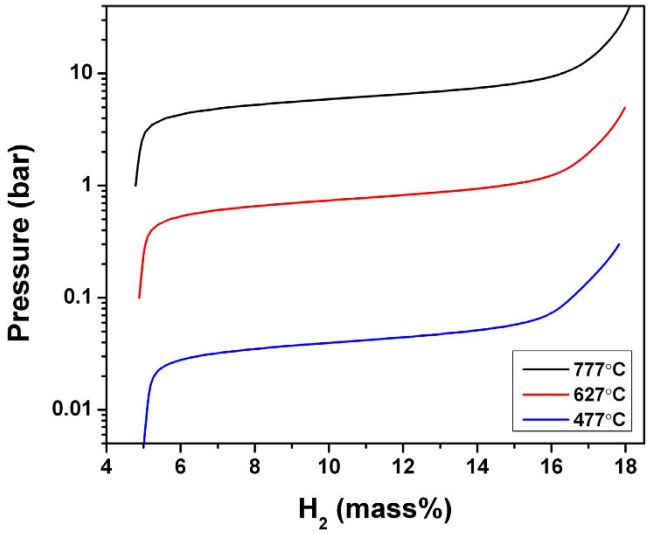

Figure 6. Calculated pressure-composition isotherms for $(LiBH_4)_6$ clusters.

with the slope arising from the intermediate steps and from the fact that the cluster probabilities p_f in Eq. S2 vary continuously with pressure and temperature. We note that sloping plateaus are seen in experimental study of pressure-composition isotherms of bulk-$LiBH_4$ [5], but this is likely due to kinetic limitations, not thermodynamic effects. Additionally, the apparent width of the plateau increases slightly with increasing temperature, which we attribute to the narrowing of the thermodynamic stability windows for the intermediate cluster compositions between $(LiBH_4)_6$ and $Li_2B_6H_6$.

Conclusions

We present a detailed computational study of the decomposition thermodynamics of small $LiBH_4$ nanoclusters using DFT-based ground state structure prediction algorithms and total DFT free energies, including vibrational contributions. With a few exceptions at very small sizes, nanoclusters favor the same decomposition sequence into closoborane $Li_2B_nH_n$ species as bulk $LiBH_4$. The calculated reaction enthalpies are higher than those for bulk materials because the total formation energies of the reaction product clusters approach their bulk values significantly slower than $(LiBH_4)_n$. Hence, reduction of cluster size is not expected to improve the thermodynamic properties of $LiBH_4$ for use in reversible hydrogen storage. Since experimental studies have demonstrated significant reduction of hydrogen release temperatures in supported nanoclusters, this confirms the importance of cluster-substrate binding energies for the thermodynamics of hydrogen release reactions. It also suggests that technologically favorable thermodynamics of $LiBH_4$ nanocluster decomposition could be engineered by varying the microscopic structure and composition of the porous substrate to lower the enthalpies of the reactants and achieve hydrogen release at temperatures compatible with the operating conditions of PEM fuel cells. Furthermore, we find that in all cases the decomposition pathways of $(LiBH_4)_2$, $(LiBH_4)_3$, and $(LiBH_4)_6$ consist of multiple intermediate stages, most of them separated by release of an integer number of H_2 molecules. While in bulk systems each reaction occurs along a sharp temperature-pressure curve given by the van't Hoff relation, in nanoclusters the transitions between the cluster phases of different compositions are smooth and characterized by broad coexistence regions on the temperature and pressure; within these regions, clusters of different compositions coexist and their equilibrium fractions vary continuously. As a result, the calculated pressure-composition isotherms exhibit sloping plateaus and smooth variation near the regions of stable bulk compositions.

Computational Methods. The structural and thermodynamic properties of small $(LiBH_4)_n$ ($n \leq 12$) clusters are studied using first-principles DFT[40,41] calculations in conjunction with state-of-the-art genetic algorithm (GA)[42–44] and prototype electrostatic ground state search (PEGS)[45] for structure predictions. The detailed descriptions of our computational methods can be found in the Supplementary Information. Decomposition pathways and pressure-composition isotherms are determined using free energy minimization in the grand canonical ensemble (see Supplementary Information).

References

1. Schlapbach, L. & Züttel, A. Hydrogen-storage materials for mobile applications. *Nature* **414,** 353 (2001).
2. Bogdanović, B. & Schwickardi, M. Ti-doped alkali metal aluminium hydrides as potential novel reversible hydrogen storage materials. *J. Alloys Compd.* **253–254,** 1 (1997).
3. Züttel, A. *et al.* $LiBH_4$ a new hydrogen storage material. *J. Power Sources* **118,** 1 (2003).
4. Orimo, S. *et al.* Dehydriding and rehydriding reactions of $LiBH_4$. *J. Alloys Compd.* **404–406,** 427 (2005).
5. Mauron, P. *et al.* Stability and Reversibility of $LiBH_4$. *J. Phys. Chem. B* **112,** 906 (2008).
6. Kostka, J., Lohstroh, W., Fichtner, M. & Hahn, H. Diborane Release from $LiBH_4$/Silica-Gel Mixtures and the Effect of Additives. *J. Phys. Chem. C* **111,** 14026 (2007).
7. Au, M. *et al.* Stability and Reversibility of Lithium Borohydrides Doped by Metal Halides and Hydrides. *J. Phys. Chem. C* **112(47),** 18661 (2008).

8. Cai, W. T., Wang, H., Jiao, L. F., Wang, Y. J. & Zhu, M. Remarkable irreversible and reversible dehydrogenation of $LiBH_4$ by doping with nanosized cobalt metalloid compounds. *Int. J. Hydrogen Energy* **38,** 3304 (2013).
9. Sun, W. W. *et al.* Nanoconfinement of lithium borohydride in Cu-MOFs towards low temperature dehydrogenation. *Dalton Trans.* **40,** 5673 (2011).
10. Si, X. L. *et al.* Metals (Ni, Fe)-Incorporated Titanate Nanotubes Induced Destabilization of $LiBH_4$. *J. Phys. Chem. C* **115,** 9780 (2011).
11. Reilly, J. J. & Wiswall, R. H. Reaction of hydrogen with alloys of magnesium and copper. *Inorg. Chem.* **6(12),** 2220–2223 (1967).
12. Reilly, J. J. & Wiswall, R. H. Reaction of hydrogen with alloys of magnesium and nickel and the formation of Mg2NiH4. *Inorg. Chem.* **7(11),** 2254–2256 (1968).
13. Siegel, D. J., Wolverton, C. & Ozoliņš, V. Reaction energetics and crystal structure of $Li_4BN_3H_{10}$ from first principles. *Phys. Rev. B* **75,** 014101 (2007).
14. Vajo, J. J. & Skeith, S. L. Reversible Storage of Hydrogen in Destabilized $LiBH_4$. *J. Phys. Chem. B* **109(9),** 3719–3722 (2005).
15. Sun, T. *et al.* Confined $LiBH_4$: Enabling Fast Hydrogen Release at ~100 °C. *Int. J. Hydrogen Energy* **37,** 18920 (2012).
16. Guo, L. J. *et al.* Enhanced desorption properties of $LiBH_4$ incorporated into mesoporous TiO_2. *Int. J. Hydrogen Energy* **38,** 162 (2013).
17. Zhang, Y. *et al.* $LiBH_4$ nanoparticles supported by disordered mesoporous carbon: Hydrogen storage performances and destabilization mechanisms. *Int. J. Hydrogen Energy* **32,** 3976 (2007).
18. Gross, A. F., Vajo, J. J., Van Atta, S. L. & Olson, G. L. Enhanced Hydrogen Storage Kinetics of $LiBH_4$ in Nanoporous Carbon Scaffolds. *J. Phys. Chem. C* **112,** 5651 (2008).
19. Fang, Z. Z. *et al. et al.* Kinetic- and thermodynamic-based improvements of lithium borohydride incorporated into activated carbon. *Acta Materialia* **56,** 6257 (2008).
20. Cahen, S., Eymery, J.-B., Janot, R. & Tarascon, J.-M. Improvement of the $LiBH_4$ hydrogen desorption by inclusion into mesoporous carbons. *J. Power Sources* **189,** 902 (2009).
21. Gosalawit-Utke, R. *et al.* Destabilization of $LiBH_4$ by nanoconfinement in PMMAcoBM polymer matrix for reversible hydrogen storage. *Int. J. Hydrogen Energy* **39,** 5019 (2014).
22. Zhang, L. T. *et al.* Superior dehydrogenation performance of nanoscale lithium borohydride modified with fluorographite. *Int. J. Hydrogen Energy* **39,** 896 (2014).
23. Ngene, P., van Zwienen, M. (Rien) & de Jongh, P. E. Reversibility of the hydrogen desorption from $LiBH_4$: a synergetic effect of nanoconfinement and Ni addition. *Chem. Commun.* **46,** 8201 (2010).
24. Li, C., Peng, P., Zhou, D. W. & Wan, L. Research progress in LiBH4 for hydrogen storage: A review. *Int. J. Hydrogen Energy* **36,** 14512 (2011).
25. Liu, X. F., Peaslee, D., Jost, C. Z. & Majzoub, E. H. Controlling the Decomposition Pathway of $LiBH_4$ via Confinement in Highly Ordered Nanoporous Carbon. *J. Phys. Chem. C* **114,** 14036 (2010).
26. Liu, X. F., Peaslee, D., Jost, C. Z., Baumann, T. F. & Majzoub, E. H. Systematic Pore-Size Effects of Nanoconfinement of $LiBH_4$: Elimination of Diborane Release and Tunable Behavior for Hydrogen Storage Applications. *Chem. Mater.* **23,** 1331 (2011).
27. Hazrati, E., Brocks, G. & de Wijs, G. A. First-Principles Study of $LiBH_4$ Nanoclusters and Their Hydrogen Storage Properties. *J. Phys. Chem. C* **116,** 18038 (2012).
28. Mason, T. & Majzoub, E.H. Effects of a Carbon Surface Environment on the Decomposition Properties of Nanoparticle $LiBH_4$: A First-Principles Study. *J. Phys. Chem. C* **118,** 8852–8858 (2014).
29. Majzoub, E. H., Zhou, F. & Ozoliņš, V. First-Principles Calculated Phase Diagram for Nanoclusters in the Na-Al-H System: A Single-Step Decomposition Pathway for $NaAlH_4$. *J. Phys. Chem. C* **115,** 2636 (2011).
30. Ozoliņš, V., Majzoub, E. H. & Wolverton, C. First-Principles Prediction of Thermodynamically Reversible Hydrogen Storage Reactions in the Li–Mg–Ca–B–H System. *J. Am. Chem. Soc.* **131,** 230 (2009).
31. Boustani, I. Systematic *ab initio* investigation of bare boron clusters:mDetermination of the geometry and electronic structures of B_n (n = 2–14). *Phys. Rev. B* **55,** 16426 (1997).
32. Nguyen, M. T., Matus, M. H., Ngan, V. T., Grant, D. J. & Dixon, D. A. Thermochemistry and Electronic Structure of Small Boron and Boron Oxide Clusters and Their Anions. *J. Phys. Chem. A* **113,** 4895 (2009).
33. Tai, T. B., Grant, D. J., Nguyen, M. T. & Dixon, D. A. Thermochemistry and Electronic Structure of Small Boron Clusters (B_n, n = 5–13) and Their Anions. *J. Phys Chem A* **114,** 994 (2010).
34. Gardet, G., Rogemond, F. & Chermette, H. Density functional theory study of some structural and energetic properties of small lithium clusters. *J. Chem. Phys.* **105,** 9933 (1996).
35. Fournier, R., Cheng, J. B. Y. & Wong, A. Theoretical study of the structure of lithium clusters. *J. Chem. Phys.* **119,** 9444 (2003).
36. Zhang, Y., Wang, Y., Michel, K. & Wolverton, C. First-principles insight into the degeneracy of ground-state $LiBH_4$ structures. *Phys. Rev. B* **86,** 094111 (2012).
37. Soulié, J-Ph, Renaudin, G., Cerný, R. & Yvon, K. Lithium boro-hydride $LiBH_4$: I. Crystal structure. *J. Alloys Compd.* **346,** 200 (2002).
38. Liu, Z. J., Qu, X. H., Huang, B. Y. & Li, Z. Y. Crystal structure and morphology of a new compound, LiB. *J. Alloys Compd.* **311,** 256 (2000).
39. Mueller, T. & Ceder, G. Effect of Particle Size on Hydrogen Release from Sodium Alanate Nanoparticles. *ACS Nano* **4,** 5647 (2010).
40. Kresse, G. & Hafner, J. *Ab initio* molecular dynamics for liquid metals. *Phys. Rev. B* **47,** 558 (1993).
41. Kresse, G. & Furthmüller, J. Efficient iterative schemes for *an initio* total-energy calculations using plane-wave basis set. *Phys. Rev. B* **54,** 11169 (1996).
42. Deaven, D. M. & Ho, K. M. Molecular Geometry Optimization with a Genetic Algorithm. *Phys. Rev. Lett.* **75,** 288 (1995).
43. Ho, K. M. *et al.* Structures of medium-sized silicon clusters. *Nature* **392,** 582 (1998).
44. Chuang, F. C., Wang, C. Z. & Ho, K. M. Structure of neutral aluminum clusters Al_n ($2 \leq n \leq 23$): Genetic algorithm tight-binding calculations. *Phys. Rev. B* **73,** 125431 (2006).
45. Majzoub, E. H. & Ozoliņš, V. Prototype electrostatic ground state approach to predicting crystal structures of ionic compounds: Application to hydrogen storage materials. *Phys. Rev. B* **77,** 104115 (2008).

Acknowledgements

FCC acknowledges support from the National Center for Theoretical Sciences (NCTS) and the Taiwan National Science Council (NSC) under grants NSC-101-2218-E110-003-MY3 and NSC-101-2112-M110-002-MY3. We are grateful to the National Center for High-performance Computing (NCHC) for computer time and facilities. VO acknowledges support from the U.S. Department of Energy, Office of Science, Basic Energy Sciences under award DE-FG02-07ER46433 and use of computing resources at the National Energy Research Scientific Computing Center (NERSC), which is supported by the U.S. Department of Energy under contract DE-AC02-05CH11231.

Author Contributions

F.C.C. and V.O. conceived and initiated the study. Z.Q.H. performed the GA calculations, W.C.C. performed the DFT calculations, and E.H.M. performed the PEGS calculations. W.C.C., F.C.C. and V.O. performed the analysis and contributed the discussions. F.C.C., W.C.C. and V.O. wrote the manuscript. All authors reviewed the manuscript.

Additional Information

Supplementary information accompanies this paper at http://www.nature.com/srep

Competing financial interests: The authors declare no competing financial interests.

How to cite this article: Huang, Z.-Q. *et al.* First-principles calculated decomposition pathways for $LiBH_4$ nanoclusters. *Sci. Rep.* **6**, 26056; doi: 10.1038/srep26056 (2016).